RSC Advances

PAPER

View Article Online
View Journal | View Issue

Cite this: *RSC Adv.*, 2025, **15**, 38378

Effect of xanthan gum on the interfacial and foam properties of an acidic sophorolipid solution: experimental and theoretical studies

Jinlu Zhong, Yanan Weng, Sensen Xie, Shuang Li and Dinghua Yu *

The interaction mechanism between surfactants and polymers has important guiding significance in the field of high-performance fluid design. However, research on the interactions between biological surfactants and microbial polysaccharides remains limited. In this paper, the effect of xanthan gum on the interfacial properties of an acidic sophorolipid solution, such as surface tension, viscosity, rheology and foam properties, was systematically studied by means of experimental and theoretical methods. The results showed that the addition of 0.1 wt% xanthan gum had little effect on the critical micelle concentration of acidic sophorolipid, and increased the contact angles of the aqueous solution with PTFE and PP. At the same time, the interaction between acidic sophorolipid and xanthan gum reduced the bulk viscosity of the xanthan gum solution. Furthermore, the shear-thinning characteristics of the mixed system did not change, but the yield value gradually decreased with increasing acidic sophorolipid concentration. Significantly, the addition of xanthan gum slightly reduced the foaming property of acidic sophorolipid but significantly improved the stability of the foam. Foam counting and image analysis showed that xanthan gum not only made the foam small and evenly distributed, but also inhibited the aggregation of foam effectively as acidic sophorolipid concentration increased. Finally, in order to reveal the molecular mechanism underlying the interaction between xanthan gum and acidic sophorolipid, DFT calculations were used to simulate their interaction. The results indicated that robust hydrogen bonding interactions involving carboxyl and hydroxyl groups exist between acidic sophorolipids and xanthan gum, thereby contributing to the enhancement of foam stability. These findings would provide useful references for biosurfactant applications in complicated formulations across diverse fields.

Received 24th July 2025
Accepted 27th September 2025

DOI: 10.1039/d5ra05360a

rsc.li/rsc-advances

1 Introduction

Biosurfactants are surface-active compounds synthesized by microorganisms during metabolic processes. They are distinguished by their exceptional interfacial activity, biodegradability, and environmental compatibility, which render them extensively applicable in various domains, including petroleum extraction, environmental remediation, food production, pharmaceuticals, and cosmetics.[1] Compared with conventional synthetic surfactants, biosurfactants present notable advantages in terms of their natural origin, sustainability, and environmental compatibility.[2–4] Sophorolipids (SLs), a representative class of glycolipid biosurfactants, are composed of a hydrophilic sophorose head and a hydrophobic fatty acid tail. These compounds typically exist in two structural forms: lactonic and acidic. The molecular structure of SLs is influenced by factors such as chain length, degree of unsaturation, and acetylation, which vary according to the fermentation substrate utilized.[5] Among these, acidic sophorolipids, characterized by the presence of a free carboxyl group at the molecular terminus, demonstrate enhanced solubility and foaming properties,[6] thereby facilitating their widespread application in foam cleaning, oil recovery, and wetting systems.[7]

However, foam systems generally encounter stability challenges, including drainage, film rupture, and coalescence, which are particularly pronounced at low concentrations. Although surfactants can facilitate foam formation by reducing interfacial tension, their capacity to stabilize the liquid film is inherently limited. Consequently, enhancing the foam stability of acidic sophorolipid has emerged as a pivotal area of research.[8]

In recent years, the integration of biopolymers and surfactants has been acknowledged as an effective strategy to enhance foam stability. Polysaccharides such as xanthan gum, carrageenan, pectin, alginates, gelatin, and gum arabic are extensively utilized in the food and cosmetic industries due to their non-toxicity, biodegradability, and favorable rheological properties. These polymers can effectively inhibit droplet aggregation and membrane rupture through electrostatic interactions and steric hindrance, thereby significantly enhancing foam stability.[9–12] Among these, xanthan gum (XG), an anionic

College of Biotechnology and Pharmaceutical Engineering, Nanjing Tech University, Nanjing 211816, PR China. E-mail: yudh@njtech.edu.cn; Tel: +86-25-58139386

polysaccharide derived from microorganisms, is recognized for its excellent solubility and high viscosity. It is commonly employed to thicken and stabilize foam systems.[13] By increasing system viscosity, enhancing liquid film strength, and regulating interfacial adsorption behavior, xanthan gum collaborates with surfactant molecules to improve the overall stability of foam systems.

Consequently, the combination of acidic sophorolipid and xanthan gum not only possesses the potential to enhance foam performance but also broadens its applicability in fields such as oil recovery, environmental remediation, and foam materials. This study aims to systematically examine the effects of the combination of acidic sophorolipid and xanthan gum on interfacial behavior, foam performance, and rheological properties. Through molecular simulations and electrostatic potential analysis, the potential synergistic mechanisms are elucidated. Comparative studies across various concentration systems provide a theoretical foundation for the development of biosurfactant–biopolymer formulations, thereby facilitating their practical application in detergents, cosmetics, and environmental engineering.

2 Experimental methods

2.1 Reagents and materials

Sodium hydroxide, sulfuric acid (98%), and dichloromethane were procured from Aladdin Regent Co., Ltd (Shanghai, China). Sophorolipids were provided by Shandong Lierkang Medical Technology Co., Ltd (Shandong, China). Xanthan gum was obtained from Sigma-Aldrich Corp (St. Louis, MO, USA). All standard solutions and samples were prepared using ultrapure water (resistivity = 18.2 MΩ cm) purified through a laboratory water purification system (Nanjing Yioud).

2.2 Methods

2.2.1 Preparation of acidic sophorolipid. Acidic sophorolipid (SL-COOH) was prepared in accordance with the methodology outlined in the literature.[14] In brief, a mixture of sophorolipids was subjected to a reaction with NaOH solution at 95 °C for a duration of 3 hours to facilitate saponification. Following the cooling of the mixture to room temperature, the pH was adjusted to 4 using concentrated sulfuric acid to promote the precipitation of free fatty acids. The mixture was subsequently extracted with ultrapure water and dichloromethane, followed by phase separation. The organic phase, which contained the product, was washed multiple times with water to eliminate salts and other water-soluble impurities, and then re-extracted with dichloromethane. Finally, the solvent was evaporated under vacuum, yielding a brown solid identified as the SL-COOH product.

2.2.2 Foam preparation and characterization. In the experiments, the concentration of XG was maintained at 0.1 wt%, while the concentration of SL-COOH was varied within the range of 0.4–12 mM to encompass values both above and below the critical micelle concentration (CMC) of SL-COOH. The concentration of SL-COOH was deliberately set significantly higher than that of XG to facilitate the examination of changes in foam properties before and after their combination.

Foam generation was conducted utilizing the double-syringe method,[15] which involves two 30 mL syringes connected by a three-way valve. One syringe contained 5 mL of foam solution, while the other contained 5 mL of air, resulting in a liquid volume fraction of 50%. The piston was oscillated back and forth 30 times to ensure thorough mixing of the air and liquid, thereby generating uniform foam. Subsequently, the foam was transferred to a 15 mL glass tube for further analysis.

The performance of the foam was evaluated based on two parameters: foam capacity (FC) and foam stability (FS). Experimental observations revealed that both pre- and post-combination foams exhibited a rapid drainage rate within the initial 5 minutes. Consequently, foam height after 5 minutes was selected as the time point for measuring foam stability. Furthermore, to provide a precise quantification of the liquid retention capacity of the foam, the liquid drainage percentage (LDP) was introduced as an additional evaluative parameter. Its calculation is as follows:

$$\mathrm{LDP}\% = \frac{V_{\mathrm{l}}}{V_{\mathrm{l0}}}. \quad (1)$$

The formulas for calculating FC and FS are as follows:[16]

$$\mathrm{FC}\% = \frac{V_{\mathrm{f0}} - V_{\mathrm{l0}}}{V_{\mathrm{l0}}} \times 100 \quad (2)$$

and

$$\mathrm{FS}\% = \frac{V_{\mathrm{f5}}}{V_{\mathrm{f0}}} \times 100. \quad (3)$$

In this context, V_{l0} signifies the initial liquid volume, V_{l} represents the volume of liquid drained per minute, V_{f0} denotes the foam volume at 0 minutes, and V_{f5} represents the foam volume at 5 minutes.

2.2.3 Surface tension. The formation and stability of foam are significantly influenced by the synergistic effects of surface tension and interfacial elasticity. A reduction in surface tension decreases the energy barrier for bubble nucleation, thereby enhancing the efficiency of bubble formation. Conversely, an increase in interfacial elasticity enhances the mechanical strength of the gas–liquid interface, effectively preventing the rupture of the liquid film and stabilizing the foam structure.[17] Surface tension curves of SL-COOH and its combination with XG were measured at room temperature utilizing the platinum ring method (Dunouyring method),[18] employing a fully automated surface/interface tensiometer (BZY100/BZY200, Shanghai Fangrui Instrument Co., Ltd). Prior to conducting the experiments, the instrument was calibrated using a standard weight and pure water (72 mN m^{-1}). The platinum ring was thoroughly cleaned with pure water and ethanol before each measurement, followed by heating with a Bunsen burner to eliminate any organic residues. The minimum surface tension and the critical micelle concentration (CMC) of SL-COOH and its combination with XG were derived from the surface tension curves.

2.2.4 Foam visualization. Micrographs of the newly generated foam were captured using a Nikon microscope (TS100) equipped with ToupView image analysis software. A small quantity of foam was injected onto a microscope slide featuring a groove, and variations in foam size were observed under 40× magnification. Foam images were recorded at 5, 10, and 20 minutes, and bubble size data at different time points were analyzed using Image J software.[19]

2.2.5 Wettability. Contact angle measurements were conducted utilizing a JC2000D2A contact angle goniometer (Shanghai Zhongchen Digital Technology Equipment Co., Ltd) within a temperature-controlled, closed environment. A consistent droplet volume of 2 μL was employed for all contact angle assessments. Polytetrafluoroethylene (PTFE) plates and polypropylene (PP) plates served as hydrophobic substrates. Surfactant solutions were prepared at concentrations of 0.4 mM, 3 mM, and 12 mM. Dynamic contact angles were recorded at 25 °C on the PTFE and PP plates. Prior to measurements, the PTFE and PP plates were thoroughly cleaned using acetone and deionized water.

2.2.6 Fluid property testing. The apparent viscosity and shear response of the samples were evaluated using a ROTAVISC LO-VI S000 rotational viscometer (IKA, Germany) and a DHR-2 rheometer (TA Instruments, USA). Viscosity measurements were conducted to obtain steady-state viscosity values under varying conditions, thereby reflecting the macroscopic flow resistance of the system. The SP-1 rotor was utilized, and the viscometer was thoroughly cleaned and dried prior to each measurement. Each experiment was replicated three times. For rheological testing, parallel plate fixtures with a diameter of 25 mm and a gap of 1 mm were employed. The sample underwent shear scanning over a specified shear rate range to determine the relationships among shear stress, viscosity, and shear rate. This approach enabled the characterization of the shear-thinning behavior and structural response characteristics of the system. By integrating both testing methodologies, the rheological behavior and viscosity evolution of the combined solution were comprehensively characterized.

2.2.7 Measurement of the zeta potential. Zeta potential measurements were conducted to characterize the surface charge properties of the systems. Zeta potential serves as a crucial parameter that reflects the surface charge and colloidal stability of particles, and it can indirectly indicate the presence of electrostatic interactions and aggregation tendencies among molecules.

Prior to measurement, all samples were diluted to the target concentration using deionized water. Measurements were performed at room temperature utilizing a Zetasizer instrument (model EEN3690, Malvern Instruments Ltd, UK). This instrument operates based on the principle of electrophoretic light scattering, which facilitates the accurate determination of the electrophoretic mobility of charged particles under an applied electric field, from which the zeta potential was subsequently calculated.

2.2.8 Molecular simulation. The structure of the system was optimized utilizing Gaussian 16. Subsequently, the optimized structure was examined for non-covalent interactions employing the independent gradient model (IGMH)[20] implemented in Multiwfn 3.8 (dev)[21] (isovalue = 0.007). Utilizing the cube files generated by Gaussian, the molecular electrostatic potential map of SL-COOH(XG) was produced. Structural visualization was conducted using VMD (version 1.9.3).[22]

2.3 Statistical analysis

Error bars indicate the standard deviations (SD), and the data are presented as the arithmetic means ± SD of three independent replicates. To evaluate statistical significance among different treatment groups, one-way analysis of variance (ANOVA) was performed, followed by the least significant difference (LSD) test for multiple comparisons at a significance level of $p < 0.05$. All statistical analyses were conducted using Origin 2021 software.

3 Results and discussion

3.1 Screening of XG concentration

To clarify the effect of XG concentration on the SL-COOH foam system, this study conducted compounding experiments with different XG concentrations of 0–0.5 wt% and 0.4 mM SL-COOH.

The results are shown in Fig. 1. The experimental findings indicate that as the XG concentration increases, foam stability exhibits a significant upward trend, especially at concentrations of 0.1 wt%, 0.3 wt%, and 0.5 wt%, where FS values reached 62.6%, 74.1%, and 82.4% respectively. By contrast, a low concentration of 0.05 wt% XG only brought a limited improvement in foam stability (FS = 35.7%), indicating that the effect of trace amounts of XG is limited. At a concentration of 0.1 wt%, FC and FS reached a relative balance, which is favorable for both foam formation and stability. Although further increasing the XG concentration can continue to enhance foam stability, the

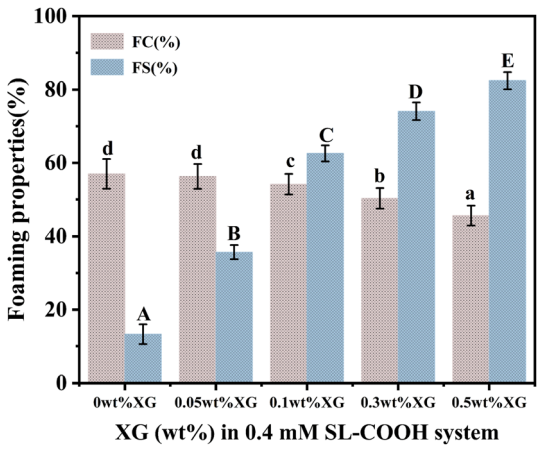

Fig. 1 Effect of different concentrations of XG on the foaming properties of 0.4 mM SL-COOH. Error bars represent the standard deviation ($n = 15$). Statistical significance was determined using one-way analysis of variance (ANOVA).

significantly increased viscosity of the system limits foam generation, with foaming ability decreasing by more than 10%.

Considering both FC and FS, 0.1 wt% XG exhibited a good synergistic stabilizing effect while exerting minimal adverse impact on foamability and was therefore selected as the representative concentration for subsequent experiments.

3.2 Surface tension

One of the key parameters of surfactant solutions is the critical micelle concentration (CMC), defined as the concentration at which the solution begins to form a substantial number of micelles.[23] The surface tension of SL-COOH and its blend with 0.1 wt% XG was measured, and a linear plot of surface tension *versus* ln C was constructed, as shown in Fig. 2A. With increasing surfactant concentration, surface tension decreased due to enhanced adsorption of surfactant molecules at the air–water interface.[24] The minimum surface tension of the SL-COOH solution was 38.2 mN m^{-1}. Upon addition of XG, the surface tension remained constant at 38.2 mN m^{-1}, indicating no change in the minimum value. Further linear fitting, as illustrated in Fig. 2B, yielded a CMC of 0.42 mM for SL-COOH, while the presence of XG slightly increased the CMC to 0.556 mM. This marginal variation suggests that under the experimental conditions, XG exerted no significant influence on the micellization behavior of SL-COOH. This observation aligns with findings reported in previous studies.[25,26]

This phenomenon may be attributed to XG, as a polysaccharide polymer, augmenting the number of hydrophilic sugar rings in the solution upon combination, which consequently diminishes the coverage of the hydrophobic groups at the oil–water interface. Therefore, a higher concentration is necessitated to achieve conditions requisite for micelle formation.

To further investigate the adsorption performance of SL-COOH, we calculated the surface excess concentration (Γ) and the cross-sectional area occupied by each SL-COOH molecule at the micelle (A) using the following formula:

$$\Gamma = -\frac{1}{nRT}\frac{d\gamma}{[d\ln c]}, \quad (4)$$

Table 1 Surface activity parameters of SL-COOH and SL-COOH-0.1 wt% XG

System	CMC (mM)	Γ (μmol m^{-2})	A (nm^2)	Minimum surface tension (γ, mN m^{-1})
SL-COOH	0.42	1.163	1.427	38.2
SL-COOH(XG)	0.556	1.098	1.513	38.2

where n is a constant that depends on the number of species present in the surfactant adsorbed at the interface, R is the gas constant (8.314 J mol^{-1} K^{-1}), γ represents the surface tension in mN m^{-1}, and T is the temperature (298 K).

The molecular area (A), measured in nm,² was calculated as follows:

$$A = \frac{1}{\Gamma \times NA} \times 10^{18}. \quad (5)$$

Based on the calculations presented in Table 1, the excess concentration (Γ) values were determined as follows: SL-COOH: 1.163×10^{-6} mol m^{-2} and SL-COOH (XG): 1.098×10^{-6} mol m^{-2}. The results for the molecular area (A) were as follows: SL-COOH: 1.427 nm^2, SL-COOH (XG): 1.513 nm^2.

The addition of XG significantly enhanced the hydrophilicity of the system, thereby increasing the likelihood of molecular dispersion in the aqueous phase and reducing adsorption at the oil–water interface. This phenomenon resulted in a decrease in the surface excess concentration. Furthermore, the presence of XG slightly augmented the molecular spacing at the interface. Additionally, the arrangement of molecules at the interface became more loosely packed, which contributed to an increase in the area occupied by the molecules at the interface. These experimental findings indicate that XG can modify the interfacial adsorption behavior of SL-COOH through weak intermolecular interactions. Such alterations may encompass changes in adsorption density, molecular arrangement, and structural properties of the interfacial layer, which in turn can significantly influence the surface and foam characteristics of the system.

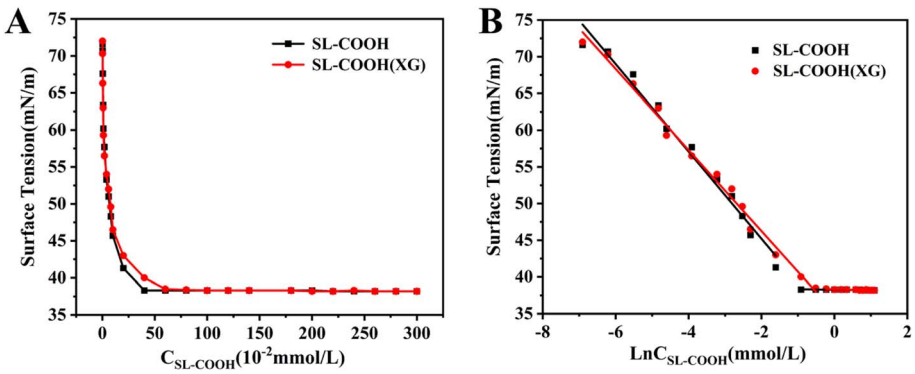

Fig. 2 Surface tension of SL-COOH and SL-COOH-0.1 wt% XG solutions. (A) Surface tension profiles; (B) linear correlation between surface tension and −ln(C).

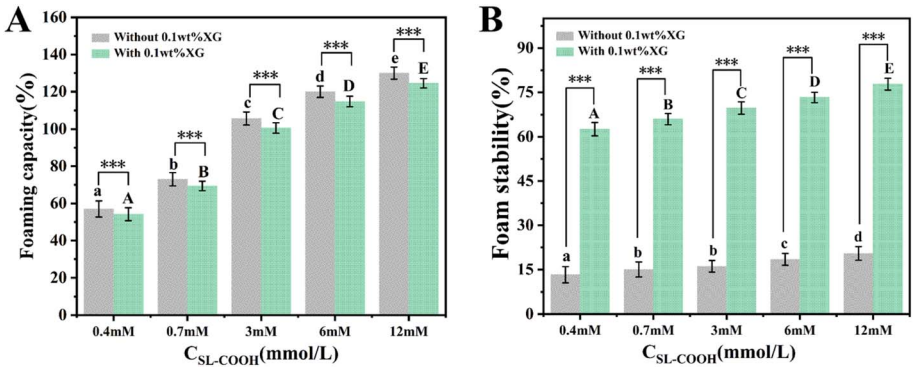

Fig. 3 Foam performance of SL-COOH solutions with or without 0.1 wt% XG at different concentrations. (A) Variations in foaming capacity and (B) foam stability. Error bars indicate the standard deviation ($n = 15$). Statistical significance was determined using one-way analysis of variance (ANOVA) compared with the no-XG group: ***$p < 0.001$.

3.3 Foam characteristics

3.3.1 Foam capacity and foam stability. Research has demonstrated that foaming surfactant solutions play an important role and have been widely studied in cleaning applications.[27] Consequently, foam was generated utilizing the double-syringe method to investigate the foaming properties of surfactant solutions.[28]

Fig. 3 illustrates that the foam capacity and foam stability of acidic sophorolipid display staged behavior in response to variations in concentration. Utilizing the critical micelle concentration (CMC) value of SL-COOH as a reference point, the incorporation of XG resulted in a reduction in foaming volume by less than 10%, with negligible effects on overall foam capacity. Nevertheless, at concentrations below the CMC, foam stability experienced an increase of 370.8%. When the SL-COOH concentration surpassed the CMC, the enhancement in foam stability plateaued, yet remained above 270%. This indicates that low concentrations of XG can substantially improve foam stability in SL-COOH systems, albeit with a slight reduction in foam capacity. Petkova *et al.*[29] experimentally investigated the effect of polymer–surfactant systems on foam properties. They found that, compared with pure surfactant solutions, mixtures of oppositely charged polymers and surfactants enhanced foam stability while reducing foaming capacity.

The adsorption data presented in Table 1 indicate that, following the addition of XG, the interfacial adsorption (Γ) of SL-COOH decreased, while the molecular area increased, resulting in a loosely packed arrangement of molecules at the interface.

The molecular migration rate at the interface has a direct impact on foam formation. The incorporation of polysaccharide polymers typically enhances the viscosity of the system, thereby improving the viscoelasticity of the foam liquid film, which in turn reduces the interfacial migration rate and inhibits foam formation.[30–33]

This finding aligns with observations reported in the literature,[34] which suggest that a decrease in the instantaneous adsorption of surfactants may lead to diminished interface coverage, consequently inhibiting foam formation. A critical mechanism underlying foam stability is foam drainage, which is intricately linked to the viscosity of the foam solution. XG enhances foam stability by increasing the viscosity and strength of the liquid film, thereby preventing bubble coalescence and improving both bubble number and distribution.[35,36]

When the concentration exceeds the critical micelle concentration (CMC), the interfacial adsorption of the system approaches saturation. At this point, additional surfactant molecules are more likely to form micelles rather than continue adsorbing at the gas–liquid interface. Meanwhile, the enhancing effect of XG on the viscoelasticity of the liquid film also reaches a plateau, resulting in no further significant increase in foam stability, although it remains at a high level. This phenomenon has already been reported in similar literature.[37]

Therefore, when incorporating XG, it is essential to carefully consider its dual effects on foamability and foam stability.

Fig. 4 further shows liquid drainage behavior, underscoring significant disparities in foam stability across the various systems. Overall, foams generated from SL-COOH solutions exhibited rapid liquid drainage within the initial 5 minutes,

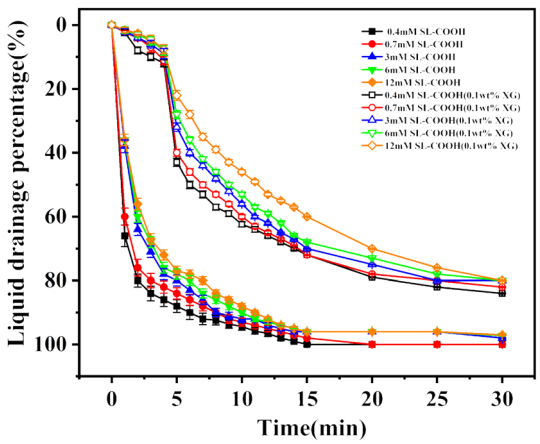

Fig. 4 Liquid drainage percentage of SL-COOH foams with and without XG at different concentrations over time. Error bars indicate the standard deviation ($n = 15$).

with nearly all liquid expelled by the 15-minute mark. This phenomenon was particularly pronounced at low concentrations, where foam films thinned rapidly due to water loss, resulting in an increased likelihood of film rupture and a swift decline in foam volume.

By contrast, the incorporation of XG significantly enhanced the liquid retention capacity of the foams. This phenomenon was particularly pronounced in the 12 mM SL-COOH system, which indicates that low foam liquid drainage volume corresponds to enhanced foam stability.[38]

This observation is consistent with the prior analysis regarding the enhanced foam stability conferred by XG. The improvement can be attributed to the substantial increase in solution viscosity, which augments the viscoelastic properties of the foam films, thereby suppressing gravitational drainage both within Plateau borders and across films. This stabilization mechanism aligns with the three-stage foam drainage theory delineated in the literature:[39] (i) an initial stage of forced drainage driven by foam injection, (ii) a gravity-controlled intermediate stage of free drainage, and (iii) a final stage of accelerated drainage induced by bubble coarsening and film rupture. In the present system, the addition of XG effectively postponed the onset of both free drainage and coarsening-induced drainage, enabling the foam to retain a high liquid content for an extended duration and thereby enhancing overall foam stability.

3.4 Foam visualization

To effectively characterize the coarsening behavior of the foam, optical microscopy was employed to monitor temporal changes in foam structure. The following characteristics were systematically analyzed: (1) variations in the number of bubbles within the field of view and (2) changes in the average bubble diameter.

3.4.1 Foam morphology changes. Fig. 5 presents micrographs of foam observed at 5 and 20 minutes post-foaming for SL-COOH solutions at varying concentrations (0.4, 3, and 12 mM), both with and without the addition of XG, captured at a magnification of 40×.

Foam coarsening results from the combined effects of Ostwald ripening and bubble coalescence.[40–43] On one hand, a Laplace pressure differential exists between bubbles of varying sizes (with small bubbles exhibiting high internal pressure), which induces the diffusion of gas from smaller to larger bubbles through the intervening liquid film (*i.e.*, Ostwald ripening). The corresponding ripening rate is expressed by eqn (6):[44]

$$\Omega = \frac{\mathrm{d}D_{\mathrm{sm}}{}^{3}}{\mathrm{d}t}. \tag{6}$$

where D_{sm} denotes the average bubble diameter, and t represents time.

Conversely, liquid film drainage results in the thinning and subsequent rupture of the liquid film, thereby promoting bubble coalescence. The thermal activation energy barrier for coalescence, which reflects the resistance of the liquid film to coalescence, can be expressed *via* eqn (7):[44]

$$W^{*} = \frac{\mathrm{d}h_{\mathrm{f}}{}^{2}\sigma_{\mathrm{h}}{}^{2}}{\gamma}, \tag{7}$$

where h_{f} is the liquid film thickness, σ_{h} is the interfacial tension at the curved pore boundary, and γ refers to the surface tension at the planar interface.

As shown in Fig. 5A, the SL-COOH foam system drains liquid relatively quickly over time, especially at the low concentration of 0.4 mM. At 5 minutes, large bubbles appear, and by 20 minutes, the bubble size increases further and becomes unevenly distributed, indicating poor system stability. With the addition of XG, the foam at the initial 5 minutes becomes

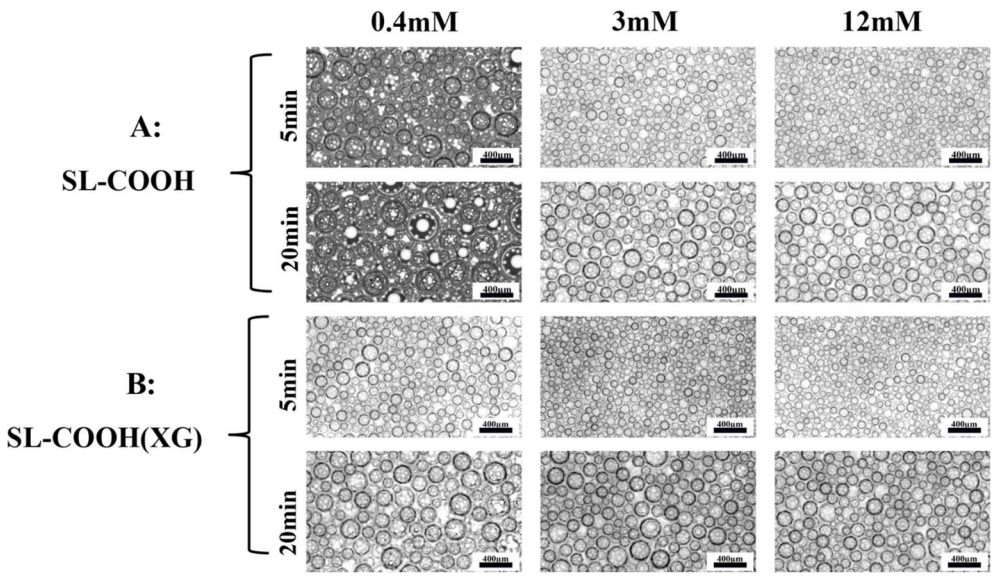

Fig. 5 Microscopic foam morphology of SL-COOH (0.4, 3, and 12 mM) recorded at 5 and 20 min. (A) SL-COOH solutions and (B) SL-COOH-0.1 wt% XG.

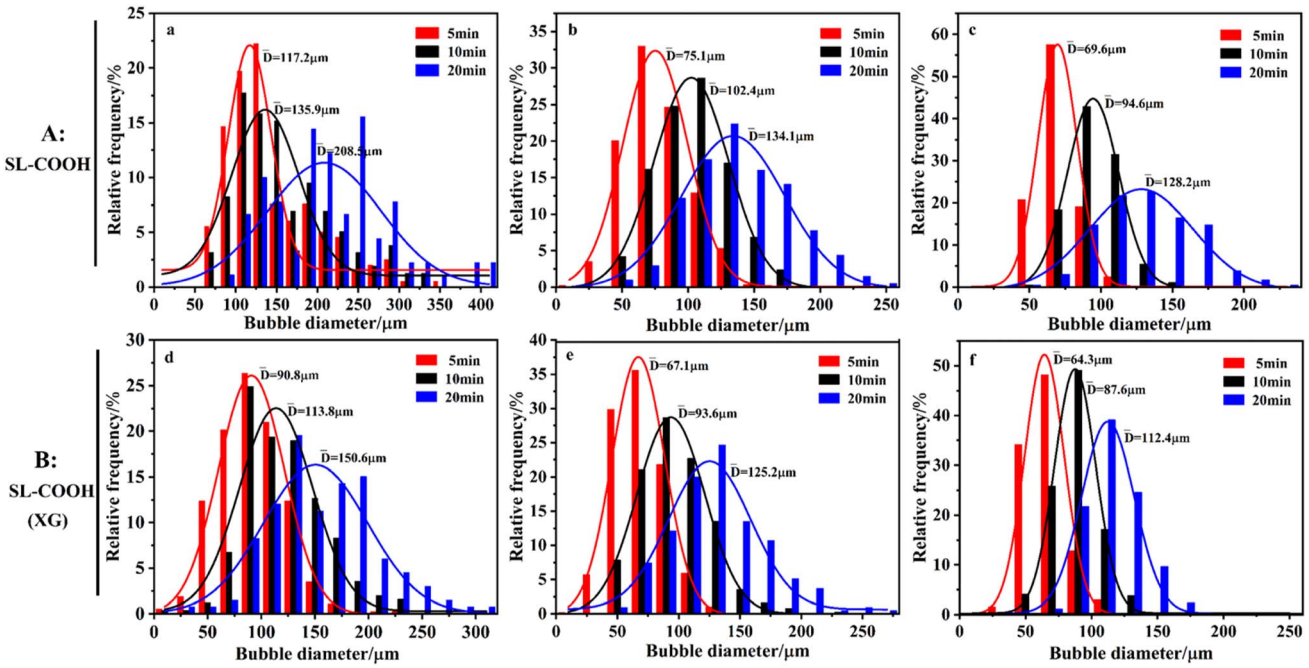

Fig. 6 Time-dependent bubble size distribution: (A) SL-COOH solutions at different concentrations (0.4, 3, and 12 mM) at 5, 10, and 20 min and (B) SL-COOH-0.1 wt% XG under the same conditions.

uniform and fine, with an even bubble distribution and improved stability.

It is hypothesized that the incorporation of XG suppresses both primary coarsening mechanisms. The polymer chains of XG significantly increase the viscosity of the system, slow the diffusion rate of gas through the liquid film, and markedly reduce the average foam diameter, thereby lowering the Ostwald ripening rate. Simultaneously, interactions between XG and the surfactant augment the liquid film thickness and interfacial viscoelasticity, thereby elevating the coalescence energy barrier W^* and rendering the liquid film resistant to rupture. Therefore, the introduction of XG reduces foam coarsening in SL-COOH alone and improves foam stability.

3.4.2 Changes in foam diameter distribution. To precisely quantify temporal variations in foam size, we employed ImageJ and ToupView software to perform statistical analyses of foam particle dimensions in the acquired micrographs.

Fig. 6A shows the initial bubble size distribution for SL-COOH alone, revealing that the bubbles formed were large. As anticipated, bubble size increased over time as a consequence of liquid drainage and coalescence. For example, in the 0.4 mM SL-COOH solution, the mean foam diameter expanded from 117.2 μm to 208.5 μm. When the concentration was elevated to 3 mM and 12 mM, the growth in bubble diameter was less pronounced, and the size distribution became narrower, implying that higher SL-COOH concentrations enhanced foam stability to a certain degree.

Following the incorporation of XG, as illustrated in Fig. 6B, the mean bubble size exhibits a marked reduction over time, accompanied by a narrowly distributed size range. This observation suggests that the presence of XG leads to an increase in system viscosity, a diminished migration rate of surfactant molecules, a reduced liquid drainage rate, and a suppression of bubble coalescence, thereby retarding the coarsening process.[45–47] These observations further corroborate the analysis of the coarsening phenomenon shown in Fig. 5.

3.5 Wettability

Surfactants are widely employed to enhance the wettability of aqueous solutions on hydrophobic surfaces.[48] Fig. 7 depicts the influence of XG incorporation on the wettability of SL-COOH solutions at varying concentrations on two hydrophobic substrates: polytetrafluoroethylene (PTFE) and polypropylene (PP).

As shown in Fig. 7A and B: the contact angles of SL-COOH solutions all decrease gradually over time; moreover, as the concentration increases, the change in contact angle tends to flatten, indicating that the substrate surface is approaching its inherent hydrophobic limit. A further comparison between different substrates reveals that the wettability of the PP plate is superior to that of the PTFE plate. This difference stems from the material properties of PTFE.[49–51] As a polymer polymerized from tetrafluoroethylene, PTFE not only possesses high thermal stability and excellent chemical stability but also has extremely low surface energy. The contact angle of water on its surface is 107°, thus resulting in inferior wettability compared with the PP plate.

Following the incorporation of XG, the contact angle of the solution exhibits a slight increase. Although this observation appears to contrast with the pronounced foam stability-enhancing effect of XG, it can be rationalized in terms of its intrinsic physicochemical properties and the nature of the intermolecular interactions involved.

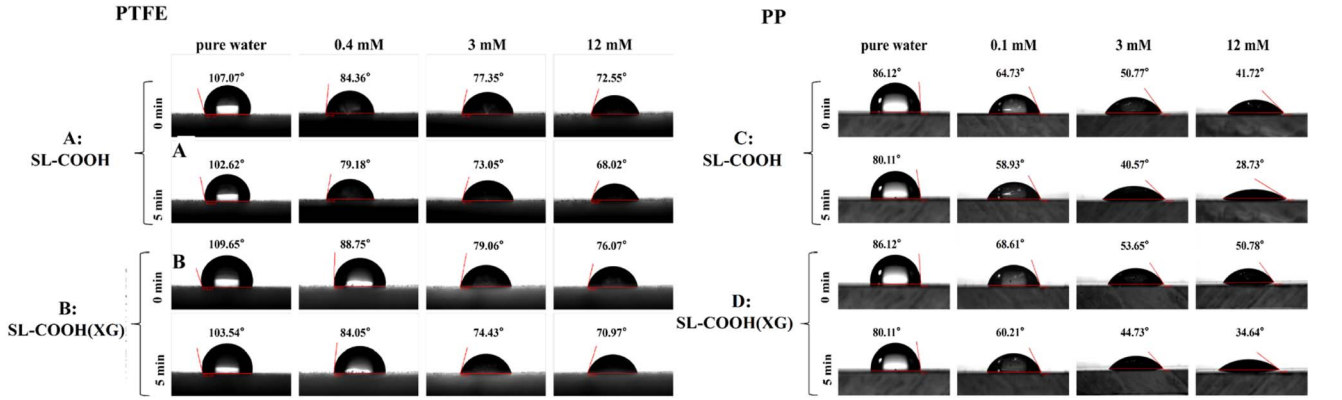

Fig. 7 Variations in contact angle of SL-COOH solutions at different concentrations (0.4, 3, and 12 mM) on two hydrophobic substrates (PTFE and PP). (A) Time-dependent contact angle of SL-COOH solution in the absence of XG on PTFE plates; (B) time-dependent contact angle of SL-COOH solution containing 0.1 wt% XG on PTFE plates; (C) time-dependent contact angle of SL-COOH solution in the absence of XG on PP plates; (D) time-dependent contact angle of SL-COOH solution containing 0.1 wt% XG on PP plates.

On one hand, the high molecular weight and extended chain conformation of XG give rise to a steric hindrance effect upon interaction with the SL-COOH surface, thereby impeding the approach of water molecules to the substrate and directly resulting in a modest increase in the contact angle.

On the other hand, both SL-COOH and XG possess hydroxyl and carboxyl functional groups within their molecular frameworks. Upon complexation, extensive intermolecular hydrogen bonding occurs, which reduces the availability of free hydroxyl and carboxyl groups in the system, thereby slightly diminishing overall hydrophilicity. This mechanism has been substantiated in the sodium alginate-krill protein system, where the introduction of graphene oxide facilitates hydrogen bond formation, similarly leading to reduced hydrophilicity and an increased contact angle.[52] Furthermore, Liang *et al.*[53] reported in their investigation of polymer–surfactant composite systems that, at elevated concentrations, van der Waals forces promote molecular aggregation, resulting in the formation of a saturated interfacial film structure. This structural arrangement inhibits further reduction of the contact angle, thereby providing an additional explanation for the aforementioned phenomenon.

In conclusion, it can be inferred that the synergistic effects of hydrogen bonding and van der Waals interactions constitute the principal factors underlying the slight increase in the contact angle observed in the SL-COOH(XG) composite solution.

3.6 Quantum chemistry and interaction mechanism analysis

3.6.1 DFT calculations. In recent years, density functional theory (DFT) calculations have increasingly emerged as a pivotal tool in the investigation of molecular interactions, owing to their distinctive advantages in elucidating intermolecular interactions. To investigate the interaction mechanism between SL-COOH and XG, DFT calculations were conducted utilizing Gaussian 16 software to analyze the hydrogen bonding, bond lengths, and binding energies between SL-COOH and XG molecules. The optimized geometries and characteristic hydrogen bonds between SL-COOH and XG are illustrated in Fig. 8A, which encompasses C–H/O (A_1, A_2, and A_5) and O–H/H (A_3 and A_4) hydrogen bonds. Specifically, the bond lengths of these hydrogen bonds are as follows: 1.83 Å (A_1), 1.84 Å (A_2), 2.39 Å (A_3), 1.96 Å (A_4), and 1.9 Å (A_5), yielding an average bond length of 1.98 Å.

In solution, the formation of hydrogen bonds is believed to significantly enhance foam stability. Generally, a shorter hydrogen bond length correlates with greater bond energy, indicating a more stable hydrogen bond interaction. Previous studies have demonstrated that the formation of short-range hydrogen bonds can strengthen intermolecular interactions at the interface, thereby improving the structural stability of the foam membrane and enhancing the durability of the foam and its resistance to rupture.[54] Table 2 presents the electronic energies and binding energies of SL-COOH, XG, and SL-COOH(XG). The binding energy (ΔE, in kJ mol^{-1}) was calculated using the following equation:

$$\Delta E = -2625.5 \times (E_{fc} - E_f - E_c),$$

where E_{fc}, E_f, and E_c represent the electronic energies of SL-COOH (XG), XG, and SL-COOH, respectively. According to the results of the DFT calculations, the binding energy is −97.2 kJ mol^{-1}, which supports the previous hypothesis and further elucidates the potential role of hydrogen bond interactions in the stability of the system.

The interactions between SL-COOH and XG were visualized utilizing the independent gradient model (IGMH) based on Hirshfeld partitioning,[55] as illustrated in Fig. 8B. The IGMH analysis distinctly elucidates the interactions within the SL-COOH (XG) system, with blue, green, and red denoting strong attraction, van der Waals forces, and strong repulsion, respectively. The findings indicate that two predominant types of interactions govern the combined system. The blue regions, indicated by arrows in the figure, are concentrated between the carboxyl group of SL-COOH and the hydroxyl group of XG, corresponding to the sign(λ_2)ρ < −0.02 range and accompanied by multiple high δginter peaks, suggesting robust hydrogen

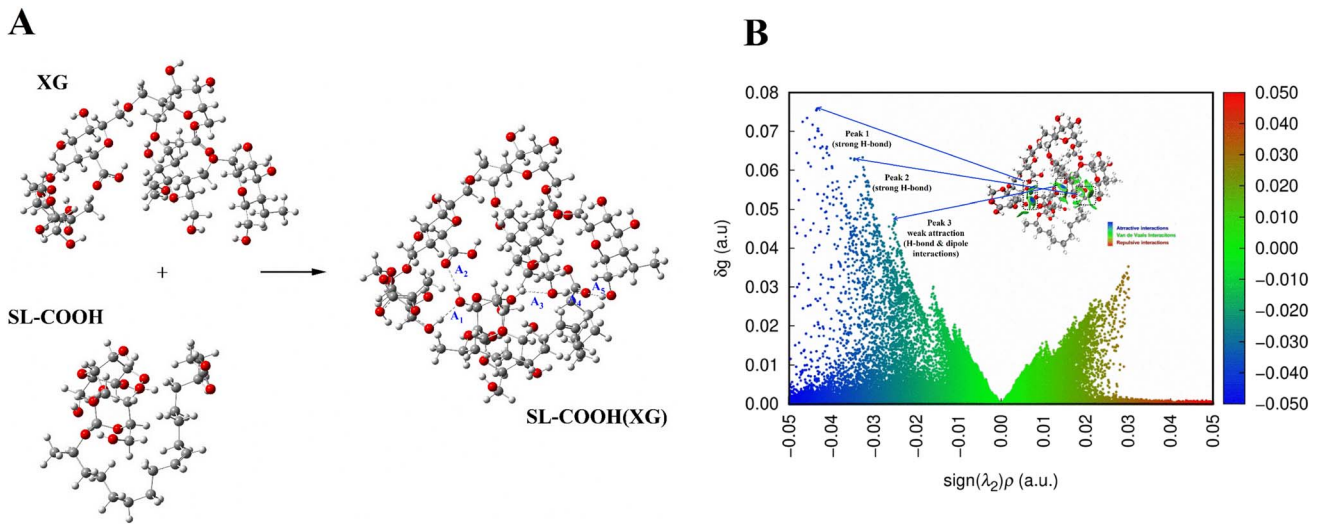

Fig. 8 (A) Molecular configurations of acidic SL-COOH, XG, and their composite system, with A1–A5 representing hydrogen bonds formed after the combination, with bond lengths of 1.83 Å (A1), 1.84 Å (A2), 2.39 Å (A3), 1.96 Å (A4), and 1.90 Å (A5); (B) IGMH isosurface and scatter plot of the SL-COOH/XG composite (isovalue = 0.007).

Table 2 Electronic energy and binding energy of SL-COOH, XG, and the SL-COOH-0.1 wt% XG complex

	Electronic energy (Hartree)	Electronic energy (kJ mol^{-1})	Binding energy (kJ mol^{-1})
SL-COOH	−2154.49	-5.65×10^6	—
XG	−4020.83	-10.55×10^6	—
SL-COOH(XG)	−6175.32	-16.21×10^6	−97.2

bond attraction between the two. This interaction contributes to the enhancement of the mechanical strength of the liquid film, thereby improving the resistance of the foam to rupture.[56] This observation is consistent with the hydrogen bond interaction sites indicated in the previous ball-and-stick model, further corroborating the existence of stable non-covalent interactions between the two.

Furthermore, the green region, corresponding to $\mathrm{sign}(\lambda_2)\rho \approx -0.01$, signifies the presence of hydrophobic van der Waals interactions within the system. As a short-range attractive force, van der Waals forces influence the aggregation and arrangement of interfacial molecules, resulting in a more loosely packed structure, which subsequently affects the wettability of the interface. This mechanism provides a plausible explanation for the observed phenomenon where the contact angle increased rather than decreased during the experiment. Overall, the IGMH analysis elucidates the non-covalent interaction characteristics of hydrogen bonds and van der Waals forces within the system, thereby aiding in the interpretation of experimental observations regarding foam stability and contact angle variations following the combination.

3.6.2 Interaction mechanisms in SL-COOH/XG rheological systems. A significant reduction in viscosity was observed when SL-COOH solutions of varying concentrations were combined with 0.1 wt% XG, as illustrated in Fig. 9A. This unexpected decrease in viscosity upon mixing a polymer with a surfactant suggests that intermolecular interactions occur between XG and SL-COOH in the solution.

Further rheological analysis, as illustrated in Fig. 9B and C, was conducted to investigate the flow behavior of the mixed systems at varying SL-COOH concentrations. As the concentration of SL-COOH increased, the apparent viscosity of the 0.1 wt% XG solution exhibited a decrease with rising shear rate, indicating that all samples displayed non-Newtonian, shear-thinning behavior (*i.e.*, pseudoplasticity). This shear-thinning phenomenon is likely attributable to hydrogen bonding or other non-covalent interactions between SL-COOH and XG molecules, which disrupt the original entangled network structure of XG. Under shear conditions, these competitive interactions result in the breakdown of the polymer network, thereby enhancing fluidity and significantly reducing the shear stress required for flow, thus demonstrating typical shear-thinning characteristics.

Changes in zeta potential serve as an indicator of the evolution of surface charge states on colloidal particles within the system.[57] As illustrated in Fig. 9D, the absolute value of the zeta potential exhibits a gradual decrease with increasing concentrations of SL-COOH, which signifies a reduction in surface charge density.

In conditions where both SL-COOH and XG are anionic, the observed charge-shielding effect is likely attributable to non-covalent interactions, such as hydrogen bonding, between SL-COOH and XG. These interactions may transpire through hydrophilic groups (*e.g.*, carboxyl and hydroxyl groups on the sugar ring), thereby facilitating the aggregation or adsorption of SL-COOH molecules around the XG polymer chains. Consequently, this leads to the shielding or attenuation of the surface charges originally present on XG, ultimately compromising the integrity of the three-dimensional network structure and resulting in a decrease in solution viscosity.

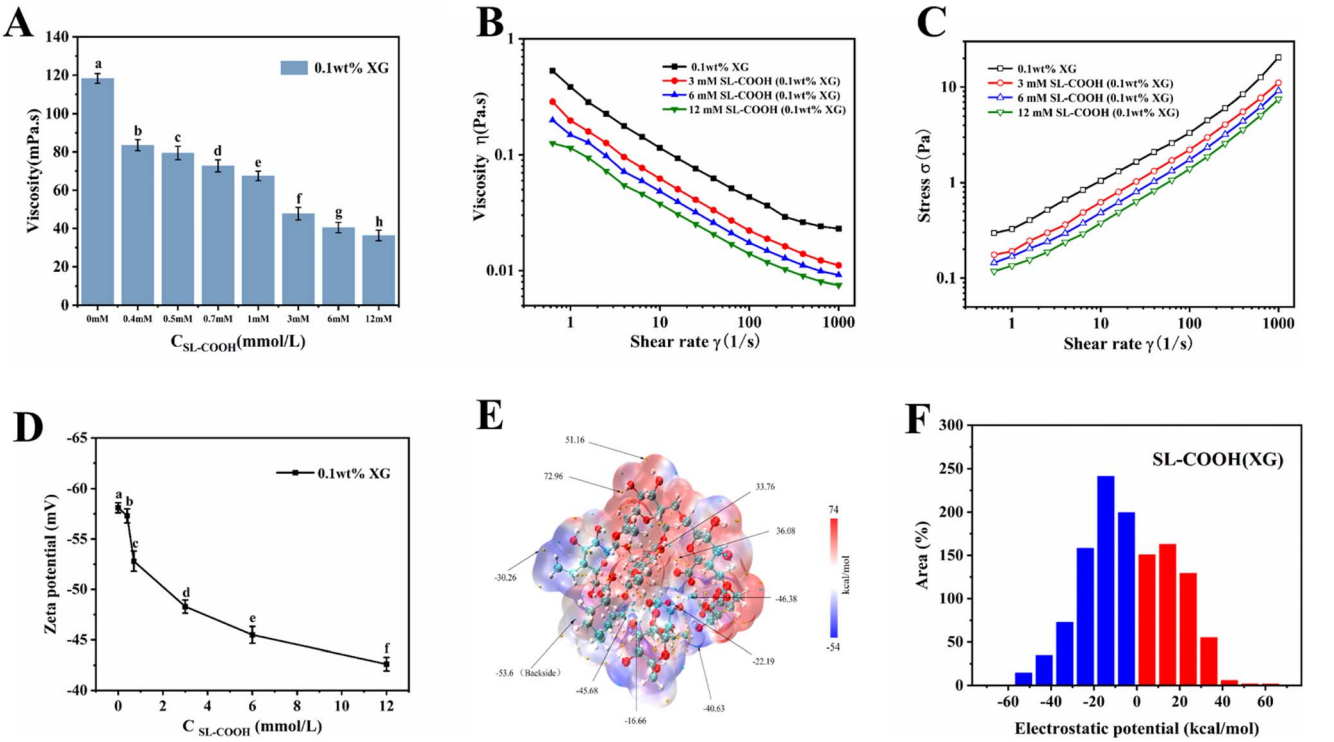

Fig. 9 (A) Viscosity changes of SL-COOH systems with and without 0.1 wt% XG at different concentrations ($n = 15$); (B) shear rate–dependent apparent viscosity and (C) shear stress of the mixed solutions; (D) zeta potential of the SL-COOH-XG mixture; (E) molecular electrostatic potential map (unit: kcal mol^{-1}); (F) histogram illustrating the distribution of electrostatic potential.

Molecular electrostatic potential (MESP) serves as an indicator of relative electron density within a molecule, thereby offering valuable insights into non-bonding interactions between molecules.[58] As illustrated in Fig. 9E and F, following the interaction between SL-COOH and XG, distinct negatively charged regions emerge on the molecular surface, constituting 58.72% of the total surface area. These regions are predominantly situated near functional groups such as carboxyl and hydroxyl, thereby confirming the overall negatively charged character of the system. The uneven distribution of these highly negative potential areas generates a polarity gradient on the molecular surface, facilitating interactions between SL-COOH and XG at multiple binding sites through hydrogen bonding and other polar interactions. This type of interaction may diminish the entanglement of XG molecular chains, disrupt their ordered arrangement, and undermine the stability of the XG network structure.

4 Conclusions

This study systematically investigates the synergistic mechanism of foam stabilization between acidic sophorolipids (SL-COOH) and xanthan gum (XG). Interestingly, their combination results in a significant decrease in viscosity, which is contrary to the commonly observed viscosity enhancement in conventional polymer–surfactant systems. Zeta potential and electrostatic potential analyses suggest that the interactions between SL-COOH and XG affect the intermolecular entanglements of XG molecular chains, inducing polymer relaxation and thereby resulting in a decrease in bulk viscosity.

Although the viscosity of the high-concentration SL-COOH system decreases to some extent, the viscosity of the SL-COOH (XG) compound system still maintains a certain level compared with that of the pure SL-COOH system, and this compound system exhibits significantly improved foam stability. Mechanistically, combined with molecular simulation results, it is found that multiple hydrogen bonds formed between SL-COOH and XG significantly enhance the interfacial viscoelasticity. This enhanced interfacial viscoelasticity can effectively inhibit liquid drainage and bubble coalescence. It is precisely this dominant enhancement effect of interfacial viscoelasticity that ultimately improves the foam stability of the SL-COOH (XG) system.

In summary, this work demonstrates that a well-structured interfacial network formed through weak intermolecular interactions can yield excellent foam stability even under low-viscosity conditions. These findings challenge the conventional view that high viscosity is a prerequisite for foam stability and provide a theoretical basis for the functional optimization of sustainable, bio-based foaming systems.

Author contributions

Jinlu Zhong: data curation, methodology, writing, review and editing. Yanan Weng: data curation, investigation. Sensen Xie: conceptualization, methodology Shuang Li: data curation,

review Dinghua Yu: supervision, data curation, project administration and funding acquisition.

Conflicts of interest

There are no conflicts to declare.

Data availability

The authors confirm that the data supporting the findings of this study are available within the article.

Acknowledgements

This work was supported by the National Key Research and Development Plan (No. 2021YFC2103800).

References

1 M. Krzan, A. Drabczyk, S. Kudłacik-Kramarczyk and M. Jamroży, Foams based on biosurfactants solutions. Part I. Influence of biosurfactant origin on foaming properties, *Curr. Opin. Colloid Interface Sci.*, 2024, **72**, 101821.
2 P. Vandana and D. Singh, Review on Biosurfactant Production and its Application, *Int. J. Curr. Microbiol. Appl. Sci.*, 2018, **7**(8), 4228–4241.
3 S. Vijayakumar and V. Saravanan, Biosurfactants-Types, Sources and Applications, *Res. J. Microbiol.*, 2015, **10**, 181–192.
4 M. Fakruddin, Biosurfactant: Production and Application, *J. Petrol Environ. Biotechnol.*, 2012, **3**(4), 1–4.
5 M. Borsanyiova, A. Patil, R. Mukherji, A. Prabhune and S. Bopegamege, Biological activity of sophorolipids and their possible use as antiviral agents, *Folia Microbiol.*, 2015, **61**, 85–89.
6 I. N. A. Van Bogaert, K. Saerens, C. De Muynck, D. Develter, W. Soetaert and E. J. Vandamme, Microbial production and application of sophorolipids, *Appl. Microbiol. Biotechnol.*, 2007, **76**, 23–34.
7 V. Shah, G. F. Doncel, T. Seyoum, K. M. Eaton, I. Zalenskaya, R. Hagver, A. Azim and R. Gross, Sophorolipids, Microbial Glycolipids with Anti-Human Immunodeficiency Virus and Sperm-Immobilizing Activities, *Antimicrob. Agents Chemother.*, 2005, **49**(10), 4093–4100.
8 S. Pal, N. Chatterjee, A. K. Das, D. J. McClements and P. Dhar, Sophorolipids: A comprehensive review on properties and applications, *Adv. Colloid Interface Sci.*, 2023, **313**, 102856.
9 M.-P. Wang, X.-W. Chen, J. Guo, J. Yang, J.-M. Wang and X.-Q. Yang, Stabilization of foam and emulsion by subcritical water-treated soy protein: Effect of aggregation state, *Food Hydrocoll.*, 2019, **87**, 619–628.
10 X. Zang, J. Wang, G. Yu and J. Cheng, Addition of anionic polysaccharides to improve the stability of rice bran protein hydrolysate-stabilized emulsions, *LWT–Food Sci. Technol.*, 2019, **111**, 573–581.
11 M. Manzoor, J. Singh, J. D. Bandral, A. Gani and R. Shams, Food hydrocolloids: Functional, nutraceutical and novel applications for delivery of bioactive compounds, *Int. J. Biol. Macromol.*, 2020, **165**, 554–567.
12 A. Yemenicioğlu, S. Farris, M. Turkyilmaz and S. Gulec, A review of current and future food applications of natural hydrocolloids, *Int. J. Food Sci. Technol.*, 2019, **54**, 1445–1456.
13 H. Zhu, L. Chen, J. Xu and Q. Han, Experimental study on performance improvement of anionic surfactant foaming agent by xanthan gum, *Constr. Build. Mater.*, 2020, **230**, 116993.
14 X. Gu, D. Li, H. Yuan, C. Li, D. Yu, G. Wang and S. Li, Tertiary/quaternary amine derivatives of sophorolipid for baicalin solubility and antioxidating performance improvement: solubilization or hydrotropy?, *J. Mol. Liq.*, 2024, **376**, 124122.
15 Z. Mitrinova, S. Tcholakova, N. Denkov and K. P. Ananthapadmanabhan, Role of interactions between cationic polymers and surfactants for foam properties, *Colloids Surf., A*, 2016, **489**, 378–391.
16 W. Li, L. Zhu, W. Zhang, C. Han, P. Li and J. Jiang, Foam and fluid properties of purified saponins and non-purified water extracts from Camellia oleifera cake (by-product), *Food Chem.*, 2024, **440**, 138313.
17 S. P. Tiwari, J. A. Steckel, M. Sarma, J. Bryant, C. A. Lippert, L. R. Widger, J. Thompson, K. Liu, N. Siefert and W. Shi, Foaming Dependence on the Interface Affinities of Surfactant-like Molecules, *Ind. Eng. Chem. Res.*, 2019, **58**(43), 19877–19889.
18 F. Hu, Y. Liu, J. Lin, W. Wang, D. H. Yu and S. Li, Acetoin modulates conformational change of surfactin: Interfacial assembly and crude oil-washing performance, *Colloids Surf., B*, 2021, **200**, 111602.
19 Z. Mitrinova, S. Tcholakova, N. Denkov and K. P. Ananthapadmanabhan, Role of interactions between cationic polymers and surfactants for foam properties, *Colloids Surf. A: Physicochem. Eng. Aspects.*, 2016, **489**, 378–391.
20 T. Lu and F. Chen, Multiwfn: A multifunctional wavefunction analyzer, *J. Comput. Chem.*, 2012, **33**, 580–592.
21 T. Lu and Q. Chen Q, Independent gradient model based on Hirshfeld partition: A new method for visual study of interactions in chemical systems, *J. Comput. Chem.*, 2022, **43**(8), 539–555.
22 W. Humphrey, A. Dalke and K. Schulten, VMD: Visual molecular dynamics, *J. Mol. Graphics*, 1996, **14**(1), 33–38.
23 J. Bergfreund, S. Siegenthaler, V. Lutz-Bueno, P. Bertsch and P. Fischer, Surfactant Adsorption to Different Fluid Interfaces, *Langmuir*, 2021, **37**, 6722–6727.
24 M. B. M. Monte and J. F. Oliveira, Flotation of sylvite with dodecylamine and the effect of added long chain alcohols, *Miner. Eng.*, 2004, **17**(3), 425–430.
25 B. Kolaric, W. Jaeger, G. Hedicke and R. v. Klitzing, Tuning of Foam Film Thickness by Different (Poly)electrolyte/Surfactant Combinations, *J. Phys. Chem. B*, 2003, **107**, 8152–8157.

26 R. Petkova, S. Tcholakova and N. D. Denkov, Role of polymer-surfactant interactions in foams: Effects of pH and surfactant head group for cationic polyvinylamine and anionic surfactants, *Colloids Surf., A*, 2013, **438**, 174–185.
27 A. Bureiko, A. Trybala, N. Kovalchuk and V. Starov, Current applications of foams formed from mixed surfactant–polymer solutions, *Adv. Colloid Interface Sci.*, 2015, **222**, 670–677.
28 W. Li, L. Zhu, F. Zhang, C. Han, P. Li and J. Jiang, Synergistic effect and performance characterization of an efficient environmental-friendly Camellia oleifera saponins based foamed cleaning agents, *J. Clean. Prod.*, 2022, **376**, 134217.
29 R. Petkova, S. Tcholakova and N. D. Denkov, Foaming and Foam Stability for Mixed Polymer-Surfactant Solutions: Effects of Surfactant Type and Polymer Charge, *Langmuir*, 2012, **28**(11), 5000–5009.
30 B. Jean and L.-T. Lee, Noninteracting *versus* interacting Poly(N-isopropylacrylamide)-surfactant mixtures at the air-water interface, *J. Phys. Chem. B*, 2005, **109**(11), 5162–5167.
31 N. Politova, S. Tcholakova, Z. Valkova, K. Golemanov and N. D. Denkov, Self-regulation of foam volume and bubble size during foaming *via* shear mixing, *Colloids Surf., A*, 2018, **539**, 18–28.
32 B. Petkova, S. Tcholakova, M. Chenkova, K. Golemanov, N. Denkov, D. Thorley and S. Stoyanov, Foamability of aqueous solutions: Role of surfactant type and concentration, *Adv. Colloid Interface Sci.*, 2020, **276**, 102084.
33 W. Yang, T. Wang, Z. Fan, Q. Miao, Z. Deng and Y. Zhu, Foams Stabilized by In Situ-Modified Nanoparticles and Anionic Surfactants for Enhanced Oil Recovery, *Energy Fuels*, 2017, **31**(5), 4721–4730.
34 B. Petkova, S. Tcholakova, M. Chenkova, K. Golemanov, N. Denkov, D. Thorley and S. Stoyanov, Foamability of aqueous solutions: Role of surfactant type and concentration, *Adv. Colloid Interface Sci.*, 2020, **276**, 102084.
35 Z. Zhang, X. Chen, C. Li, H. Feng, H. Yu, R. Zhu and T. Wang, Foam sclerotherapy during shunt surgery for portal hypertension and varices, *Open Med.*, 2017, **12**(1), 384–390.
36 W. Kang, L. Yan, F. Ding and Z. Xu, Effect of polysaccharide polymers on the surface and foam properties of aqueous film-forming foam, *Colloid Interface Sci.*, 2021, **45**, 100540.
37 H. Emami, A. Ayatizadeh Tanha, A. Khaksar Manshad and A. H. Mohammadi, Experimental Investigation of Foam Flooding Using Anionic and Nonionic Surfactants: A Screening Scenario to Assess the Effects of Salinity and pH on Foam Stability and Foam Height, *ACS Omega*, 2022, **7**, 14832–14847.
38 Y. Xiong, B. Li, C. Chen and Y. Zhang, Properties of foamed concrete with $Ca(OH)_2$ as foam stabilizer, *Cem. Concr. Compos.*, 2021, **118**, 103985.
39 Y. Sheng, S. Lu, N. Jiang, X. Wu and C. Li, Drainage of aqueous film-forming foam stabilized by different foam stabilizers, *J. Dispersion Sci. Technol.*, 2017, **39**(9), 1266–1273.
40 W. Kang, Y. He, Z. Li, H. Yang, Z. Ye, W. Li, H. Jiang, D. Liu, H. Ding and S. Turtabayev, Stability mechanisms of viscoelastic zwitterionic-anionic surfactants enhanced foam system for low-permeability reservoirs, *J. Mol. Liq.*, 2023, **369**, 120883.
41 N. Hu, Y. Li, Z. Wu, K. Lu, D. Huang and W. Liu, Foams stabilization by silica nanoparticle with cationic and anionic surfactants in column flotation: Effects of particle size, *J. Taiwan Inst. Chem. Eng.*, 2018, **88**, 62–69.
42 D. Joshi, D. N. Ramesh, S. Prakash, R. K. Saw, N. K. Maurya, K. B. Rathi, S. Mitra, O. P. Sinha, P. K. Bikkina and A. Mandal, Formulation and characterisation of polymer and nanoparticle-stabilized anionic surfactant foam for application in enhanced oil recovery, *Surf. Interfaces*, 2025, **56**, 105615.
43 Z. Briceño-Ahumada and D. Langevin, On the influence of surfactant on the coarsening of aqueous foams, *Adv. Colloid Interface Sci.*, 2017, **244**, 124–131.
44 Z. Xue, A. Worthen, A. Qajar, I. Robert, S. L. Bryant, C. Huh, M. Prodanović and K. P. Johnston, Viscosity and stability of ultra-high internal phase CO_2-in-water foams stabilized with surfactants and nanoparticles with or without polyelectrolytes, *J. Colloid Interface Sci.*, 2016, **461**, 383–395.
45 X. Dong, H. Liu, C. Wang, C. Lu and F. Yan, The polymer-enhanced foam injection process: An improved-oil-recovery technique for light oil reservoirs after polymer flooding, *Energy Sources, Part A*, 2016, **38**, 354–361.
46 D. Joshi, D. N. Ramesh, S. Prakash, R. K. Saw, N. K. Maurya, K. B. Rathi, S. Mitra, O. P. Sinha, P. K. Bikkina and A. Mandal, Formulation and characterisation of polymer and nanoparticle-stabilized anionic surfactant foam for application in enhanced oil recovery, *Surf. Interfaces*, 2025, **56**, 105615.
47 H. Zhu, L. Chen, J. Xu and Q. Han, Experimental study on performance improvement of anionic surfactant foaming agent by xanthan gum, *Constr. Build. Mater.*, 2020, **230**, 116993.
48 B. Bera, O. Carrier, E. H. G. Backus, M. Bonn, N. Shahidzadeh and D. Bonn, Counteracting Interfacial Energetics for Wetting of Hydrophobic Surfaces in the Presence of Surfactants, *Langmuir*, 2018, **34**, 41.
49 D. Mańko, A. Zdziennicka and B. Jańczuk, Surface tension of polytetrafluoroethylene and its wetting by aqueous solution of some surfactants and their mixtures, *Appl. Surf. Sci.*, 2017, **392**, 117–125.
50 Y. Huang, Q.-L. Huang, H. Liu, C.-X. Zhang, Y.-W. You, N.-N. Li and C.-F. Xiao, Preparation, characterization, and applications of electrospun ultrafine fibrous PTFE porous membranes, *J. Membr. Sci.*, 2017, **523**, 317–326.
51 Y.-Y. Peng, F. Lu and Q.-X. Tong, One-step synthesis, wettability and foaming properties of high-performance non-ionic hydro-fluorocarbon hybrid surfactants, *Appl. Surf. Sci.*, 2018, **433**, 264–270.
52 R. Zhang, J. Guo, M. Zhao, J. Wu, S. Zhang and Y. Yu, Effect of graphene oxide on the molecules of a sodium alginate-krill protein composite system and characterization of the system's composite fiber morphology and mechanical properties, *J. Appl. Polym. Sci.*, 2018, **135**(22), 46642.

53 M. Liang, X. Zhao, J. Wang and Y. Feng, A Comparative Study on CO_2-Switchable Foams Stabilized by C_{22}- or C_{18}-Tailed Tertiary Amines, *Molecules*, 2023, **28**(6), 2567.
54 C. Stubenrauch, M. Hamann, N. Preisig, V. Chauhan and R. Bordes, On how hydrogen bonds affect foam stability, *Adv. Colloid Interface Sci.*, 2017, **247**, 435–443.
55 T. Lu and Q. Chen, Independent gradient model based on Hirshfeld partition: A new method for visual study of interactions in chemical systems, *J. Comput. Chem.*, 2022, **43**(8), 539–555.
56 M. Kumar, A. Thakur, U. K. Mandal, A. Thakur and A. Bhatia, Foam-Based Drug Delivery: A Newer Approach for Pharmaceutical Dosage Form, *AAPS PharmSciTech*, 2022, **23**, 244.
57 R. Prathapan, R. Thapa, G. Garnier and R. F. Tabor, Modulating the zeta potential of cellulose nanocrystals using salts and surfactants, *Colloids Surf., A*, 2016, **509**, 11–18.
58 K. R. Raghi, D. R. Sherin, M. J. Saumya, P. S. Arun, V. N. Sobha and T. K. Manojkumar, Computational study of molecular electrostatic potential, docking and dynamics simulations of gallic acid derivatives as ABL inhibitors, *Comput. Biol. Chem.*, 2018, **74**, 239–246.